Desalination and Water Treatment
www.deswater.com

doi:10.5004/dwt.2019.24451

164 (2019) 249–262
October

Evaluation of magnetic ZSM-5 composite performance in 2, 4 dichlorophenol removal from synthetic solutions: response surface method (RSM) modeling and isotherm, kinetic and thermodynamic studies

Mohammad Darvishmotevalli[a], Mehdi Salari[b], Maryam Moradnia[a], Maryam Heydari[c], Ghasem Kiani[a], Saeid Fadaei[a], Hossein Karimi[a], Bijan Bina[a,*]

[a]*Student Research Committee, School of Health, Isfahan University of Medical Sciences, Isfahan, Iran, email: Mohamad.darvish68@gmail.com (M. Darvishmotevalli), moradnia.mui@gmail.com (M. Moradnia), ghasem_kia@yahoo.com (G. Kiani), saed_f5@yahoo.com, (S. Fadaei), h.karimi.m90@gmail.com (H. Karimi), bbina123@yahoo.com (B. Bina)*
[b]*Department of Environmental Health Engineering, School of Public Health, Hamadan University of Medical Sciences, Hamadan, Iran, email: msalari_22@yahoo.com (M. Salari)*
[c]*Department of Environmental Health Engineering, School of Public Health, Tehran University of Medical Sciences, Tehran, Iran, email: vida1heydari@gmail.com (M. Heydari)*

Received 12 January 2019; Accepted 22 May 2019

ABSTRACT

2,4-Dichlorophenol (DCP) is a chlorinated derivative of phenol that causes harmful effects on human health even at low its concentrations. The aim of this study was to investigate the adsorption of the compound from synthetic wastewater by magnetic ZSM-5 (ZSM-5/M) composite in a laboratory scale, in a batch system. The SEM, XRD and EDX analyses were used to evaluate the quality characteristics of ZSM-5/M composite. The variables effect of pH, contact time (min), dose of ZSM-5/M (g/L) and pollutant concentration (mg/L) was investigated on the adsorption process under surface response method (RSM) at 5 levels during 30 experiments. In order to measure the DCP concentration, Perkin Elmer LAMBDA 25 UV/Vis spectrophotometer was used at 580 nm wavelength. Isotherm, kinetic and thermodynamic studies of adsorption process were also performed in the optimal conditions of the variables. Diagnostic analyses showed the ZSM-5/M was successfully synthesized. At the optimum level of pH, contact time, ZSM-5/M dose, and DCP concentration to be 6.3, 120 min, 1 g/L and 10 mg/L respectively, the maximum efficiency was obtained about 96%. The adsorption process followed Freundlich isotherm (R^2 = 0.9967) and pseudo-first-order kinetic (R^2 = 0.9996), and the adsorption capacity was determined to be nearly 87.7 mg/g. Thermodynamic study illustrates that adsorption process has a spontaneous and exothermic nature. Owning to high efficiency, appropriate adsorption capacity, low cost, and the easy separation,regeneration, and reuse of the adsorbent after the adsorption process, ZSM-5/M can be potentially suggested to be applied as a promising adsorbent in the adsorption of DCP and similar compounds from aquatic environments.

Keywords: Phenol; Simulated wastewater; Adsorption process; Freundlich isotherm; Pseudo-first-order kinetic; Exothermic nature

*Corresponding author.

1. Introduction

Phenolic compounds like Chlorophenols, Nitrophenols, and Aminophenols are among chemical materials used extensively in oil refineries and various industries such as the plastics, paper, and pesticides industries [1]. Toxicity of the industrial wastewaters containing the phenolic compounds was evaluated extensively by biological tests [2–4]. Chlorophenols are toxic compounds with high COD values and low biodegradability rates that even at low concentrations, have harmful effects on living organisms and human beings [5,6]. The most common chlorophenols with a great application in industrial scale include 4-chlorophenol, 2,4-dichlorophenol, and 2,4,6-trichlorophenol [7]. 2,4-dichlorophenol (DCP), one of the very toxic chlorophenols, is characterized by solid form, colorless crystals and high solubility in alcohols, at room temperature [8]. DCP is mostly used in producing insecticides and pesticides and is employed as very important compounds in manufacturing products, such as antiseptics and disinfectants [9]. The EPA recommends that DCP concentrations in drinking water should not exceed 0.03 mg/l [10]. The World Health Organization (WHO) recommends 1 µg/L concentration as maximum permissible level of DCP in drinking water and 1 mg/L in wastewaters discharged into surface water resources [11]. Various removal methods like biological processes, chemical oxidation, extraction by solvents, reverse osmosis, electrochemical and irradiation techniques have been employed for removal of phenols and phenolic compounds from aquatic environments [12–15]. Most of these methods have shortcomings such as high costs, low efficiency, need to pre-treatment before the main treatment process, and production of by-products [16,17]. Adsorption processes are superior to other treatment methods in initial costs, wastewater reuse, design simplicity and flexibility, easy operation, insensitivity to contaminants, and toxic compounds. Adsorption has the added advantage of producing high-quality wastewater, without need to hazardous materials such as ozone and free radicals [18–26]. Nowadays, researchers are searching for natural adsorbents like rice bran, coconut husk, ash, sawdust, clay, etc. for adsorption processes, being cost-effective and high adsorption efficiency [27–29]. Al-Qodah et al. [29] reported that acid treated oil shale ash can achieve the adsorption capacity of 11.4 mg/g of pesticide deltamethrin in aqueous solutions. Qodah et al. [30] found diatomaceous silica with the maximum loading capacity of 126.6 mg/g for methylene blue in aqueous environments. As low-cost molecular sieve, membrane, and ion exchanger with catalytic properties, zeolites are promising adsorbents with widespread applications in the treatment of industrial wastewaters [31]. Yousef et al. [32] reported that natural zeolites removed phenols, with adsorption capacity of 23.3, 23.8, 24.9, and 35.5 mg/l at various temperatures of 25, 35, 45, and 55°C, respectively, and the adsorption process followed the Freundlich isotherm. In the study by Wang et al. [33], the adsorption capacity of the natural zeolite for removal of rhodamine B and methylene blue was obtained as 0.0079 and 0.0228 mmol/g, respectively. Due to the suitable features of zeolites in the adsorption process, the ZSM-5 as synthesized zeolite was used as an adsorbent in the present research. One of the main problems of the adsorption process is the separation of an adsorbent from reaction solution at the end of any experiment. Despite problems like energy loss, labor requirement, and costs, filtration and centrifugation methods are employed as common separation techniques. In the present study, the zeolite was magnetized, and separation was carried out using a magnet to simplify the separation process and diminish costs. Azari et al. [34] studied 2, 4-DCP removal from aqueous solutions using magnetized graphene oxide nanoparticles, which isolated easily and conveniently using a magnet. The first purpose of this work was to synthesize and characterize magnetic zeolite composite (ZSM-5/M). Performance of ZSM-5/M in the adsorption of DCP from synthetic wastewater was chosen as the second aim in the present study. The effect of pH, contact time, adsorbent dose, and DCP concentration parameters on adsorption performance was investigated, modeled, and optimized by using response surface methodology (RSM) based on central composite design (CCD). Use of the RSM approach has advantages like simplicity, minimizing the number of samples used in the experiment, and reducing required time, labor, and costs [35–37]. Finally, kinetic, isotherm and thermodynamic studies were also carried out at the optimum conditions of the input variables.

2. Materials and methods

2.1. Materials

The used materials in the present research, including hydrochloric acid (1 N HCl), sodium hydroxide (1 N NaOH), aluminum silicate, silica, tetrapropylammonium hydroxide (TPAOH 40% solution in H_2O), tetraethyl orthotitanate (TEOT) (97% purity), isopropanol (70% in H_2O), ferric chloride ($FeCl_3{\cdot}6H_2O$, 97%), ferrous chloride ($FeCl_2{\cdot}4H_2O$, 99%), and DCP (99% purity), were of laboratory grade and was supplied from Sigma-Aldrich.

2.2. ZSM-5 synthesis

To synthesize ZSM-5, the procedure that was clearly explained in the study of Wan and et al. was applied in the present study [38].

2.3. Synthesis and characterization of ZSM-5/M

In this stage, the synthesized zeolite was dissolved in 400 ml of a solution containing $FeCl_3$ (28 mmol) and $FeSO_4$ (14mmol) at 70°C to be magnetized. Then 100 ml of the NaOH solution (5 mol/L) was added slowly and dropwise to the solution for precipitation of the magnetic composite. The zeolite contribution was adjusted to obtain the zeolite/iron oxide weight ratio of 3:1 in order to prevent reduction of adsorption capacity. The obtained material was dried for three hours in an oven at 100°C. Physical and chemical features of the synthesized composite were characterized using scanning electron microscopy equipped with energy-dispersive X-ray spectroscopy (SEM/EDX, Cam Scan, MV2300 model). BET surface area based on N_2 adsorption/desorption method was done by a Micromeritics/Gemini-2372 surface area analyzer. The crystalline phases of ZSM-5/M were evaluated by X-ray diffraction (XRD, Rigaku miniFlex diffractometer device). The mag-

netization intensity of the magnetic *ZSM-5/M* was characterized using vibrating sample magnetometer (VSM 7400 Model Lake-Shore).

2.4. Adsorption experiments

All experiments were conducted in a laboratory scale in a 200 ml reactor with a batch system. A stock solution 0.1% (100 mg/L) was used to prepare the required concentrations. The variables of contact time, pH, DCP concentration, and ZSM-5/M dose variables are examined in the adsorption process at the levels as presented in Table 1. All the samples were exterminated in the volume of 100 ml. A 1.2 Tesla magnet was used to separate the ZSM-5/M and the remaining DCP was evaluated using a spectrophotometer (Perkin Elmer LAMBDA 25 UV/Vis) at 580 nm. A pH meter (Kent EIL 7020) was employed to adjust pH value.

2.5. Design of the experiments

RSM method based on CCD technique was used to design the experiments with a minimal number, which reduces costs and utilized materials and determines the effect of each input variable on the adsorption performance (the experiments were designed using Design-Expert version 7). Based on CCD technique, the 4 variables at 5 levels were entered into the design, as shown in Table 1, and finally, 30 experiments were provided as given in Table 3, in which 16 experiments were related to factorial points ($\alpha \pm 1$), 8 to axial points, and 6 to repetitions of the experiments in the center point ($\alpha = 0$).

To express the empirical relationship between the input variables and removal efficiency, the experimental removal efficacy was fitted to a second order polynomial equation:

$$Y = a_0 + \sum a_i x_i + \sum a_{ii} x_i^2 + \sum a_{ij} x_i x_j + \varepsilon \quad (1)$$

where Y represents the predicted removal percentage, a_0, ai, aii and aij are devoted to constant, linear, quadratic, and interactive values of regression coefficients, respectively. Also, ε and x term are related to the residual term and coded variables, respectively, and subscript i specifies the kind of variables. Eqs. (2) and (3) were used to determine adsorption efficiency and adsorption efficiency, respectively, where q is the adsorption capacity (mg/g), M is the adsorbent mass (g), V is the sample volume (L), C_0 is the initial DCP concentration (mg/L), C_e is the DCP concentration at equilibrium(mg/L), and E is the removal efficiency (%).

$$q_e = (C_0 - C_e) \times \frac{V}{M} \quad (2)$$

$$E = \frac{C_0 - C_e}{C_0} \times 100 \quad (3)$$

2.6. Adsorption isotherm, kinetics, and thermodynamic studies

After determining the optimum conditions for the studied variables, isotherm studies were carried out to investigate how the pollutant was adsorbed on the adsorbent and the adsorption capacity of the adsorbent. Isotherm studies were performed using the mathematical equations of Freundlich, Langmuir, and Temkin isotherms under optimum conditions of contact time, pH, and adsorbent dose and various phenol concentrations. Kinetic studies were carried out to determine adsorption rate constant and adsorption type by using pseudo-first-order, pseudo-second order, and inter-particle penetration models under optimum conditions of phenol concentration, adsorbent dose, and pH and different contact times. Finally, thermodinal study was performed to reveal the effect of solution temperature in the process efficiency and to specify the adsorption nature in the term of being exothermic or endothermic

3. Results

3.1. SEM and BET analyses for ZSM-5 and ZSM-5/M

SEM analysis was used to study morphological and surface features ZSM5/M. at 10 kV under 50KX magnification. As depicted in Fig. 1, ZSM-5/M particles had a cubic crystal structure that provided a good adsorption surface. Also, ZSM-5/M structure did not change as a result of magnetization, but the accumulation of ZSM_5 particles increased in the magnetic state. This can be due to synthesis of the ZSM_5in the presence of Fe_2O_3 nanoparticles. As confirmed by the BET analysis, this accumulation very probably results in a decrease in specific surface area [39]. The BET analysis was performed at 77K to determine the specific surface area and pore volume of ZSM-5 and ZSM-5/M, as related results are presented in Table 2. This table indicates that the specific surface area of ZSM-5 declined from 521.5 to 462.3 m^2/g after magnetization.

3.2. XRD analysis for ZSM-5 and ZSM-5/M

An XRD analyzer with Cu anode, operating at 40 keV and 35 mA, was used to perform XRD analysis in order to identify the crystal structure of the synthesized adsorbent

Table 1
Independent variables and the levels of each variable

Variable	Symbol	–2	–1	0	1	2
pH	X_1	3	5	7	9	11
Contact time (min)	X_2	10	37.5	65	92.5	120
Adsorbent dose	X_3	0.2	0.4	0.6	0.8	1
2,4 Dichlorophenol concentration (mg/L)	X_4	10	32.5	55	77.5	100

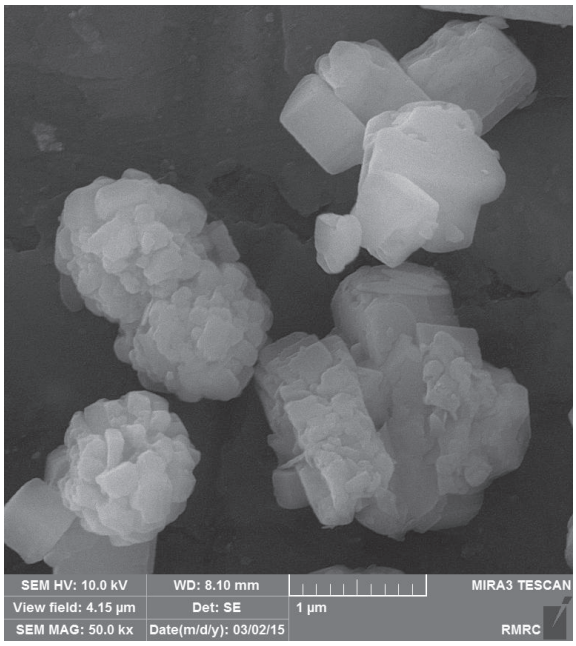

Fig. 1. SEM analysis for ZSM-5/M.

Table 2
BET analysis for ZSM-5,ZSM-5/M

Parameter	ZSM-5	ZSM-5/M
Specific surface area (m^2/g)	521.5	462.3
Total pore volume (cm^3/g)	0.3654	0.3148
Diameter average porosity (nm)	2.563	2.122

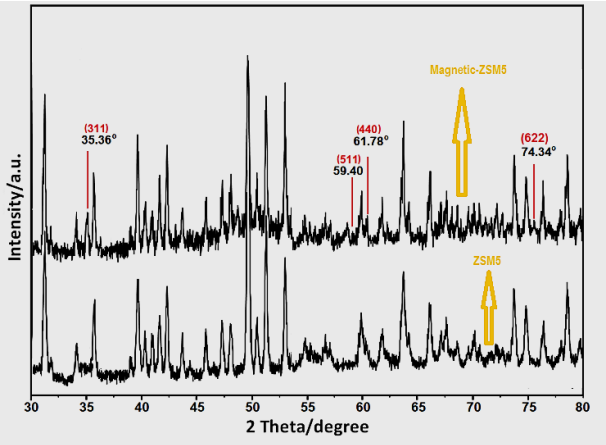

Fig. 2. XRD analysis for ZSM-5,ZSM-5/M.

at 2θ = 30–80 degrees. Results of the XRD analysis in Fig. 2 indicate that the crystal structure of ZSM-5 did not change substantially after magnetization and was stable. Only the peaks at the 2θ of 35.36, 59.40, 61.78, and 74.34, are related to the Fe_3O_4 nanoparticles in the ZSM-5/M composite, belonging to the 311, 511, 44, and 662 crystal planes of the Fe_3O_4 nanocrystals, respectively [40,41].

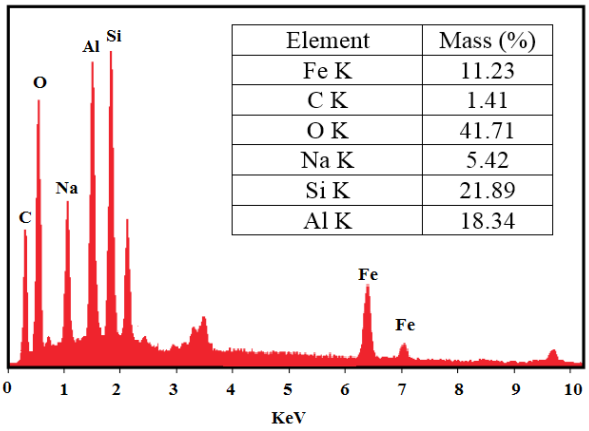

Fig. 3. EDX analysis for ZSM-5/M.

The Debye-Scherrs formula given in Eq. (4) was used to determine the average crystallite size of the ZSM-5/M particles.

$$D = \frac{K\gamma}{\beta \mathrm{Cos}\theta} \quad (4)$$

where D demons the average crystallite size, K is devoted to the shape factor (0.9), γ presents the wavelength of Cok radiation, θ is the angle of reflection and β indicates full width at the half maximum height of the peak. The average crystallite size of the ZSM-5/M was calculated to be 26.8 nm.

3.3. EDX analysis for ZSM-5 and ZSM-5/M

Fig. 3 shows the percentage of elements present in the structure of ZSM-5/M, which was determined in the EDX analysis. As shown in the figure, the elements of carbon, oxygen, sodium, aluminum, silicon, and iron are present in the structure of this composite, and oxygen composites the largest contribution in the structure. Presence of iron in the structure indicates that the ZSM-5/M composite was desirably synthesized.

3.4. VSM analysis for ZSM-5/M

VSM analysis was done in magnetic fields within ±10 KOe, as displayed in Fig. 4. The results indicate that the maximum saturation magnetization for ZSM-5/M is about up to 24 emu/g. In addition, the separation of magnetic chitosan from the reaction sample was successfully achieved after holding the sample near 1.2 tesla magnetic for 25 s.

3.5. Statistical analysis and model fitting

Experimental and predicted values for DCP adsorption by ZSM-5/M are listed in Table 3. As shown in this table, the predicted values were obtained from a second order model fitted to the experimental removal efficiency over ANOVA analysis. The F-value and p-value for this model were observed to be 619.4 and $p < 0.001$, respectively (Table 4). Moreover, most terms included to model were statistically significant. As seen in Table 4, the R^2 value was

equal to 0.9983, which suggests the high predictive ability of the model, because 99.83% of the variation in DCP removal could be predicted by this model. Furthermore, the

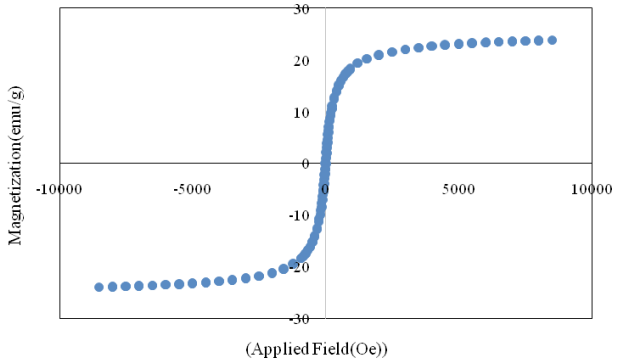

Fig. 4. VSM curve of ZSM-5/M.

value of Adj-R^2 was obtained as 0.9967, which is very close to R-squared, illustrating the high goodness of the model to fit. "Lack of fit" statistic displayed a p-value > 0.9714, so no statistically significant was obtained for it. Therefore, the first condition of lack of fitness of the model is rejected, which suggests that the model shows a good fit.

The adequacy of the fitted model was also tested through diagrams of the distribution of the residuals. Fig. 4a shows the distribution of the residuals on a straight line against the percentages. As shown in this figure, the residuals lie on this line and/or close to it, and as we get closer to the central part of the line, residuals percentage increase. This type of distribution suggests a normal distribution of residuals. Fig. 4b presents the residuals against the predicted values. About half of the residuals lie above the line and the other half below it. This distribution demonstrates that the mean of these values is close to zero and changes in the residuals do not follow a certain pattern and confirm model adequacy [42].

Table 3
Design of the experiments and experimental and predicted efficiencies of DCP adsorption by ZSM-5/M

Exam No.	pH	Time (min)	Adsorbent dose (g/L)	Contaminant concentration (mg/L)	Actual efficiency (%)	Predicted efficiency (%)
1	9	37.5	0.4	77.5	50	50.33
2	9	37.5	0.4	32.5	62	61.79
3	5	37.5	0.4	32.5	59	59.67
4	5	37.5	0.4	77.5	46	45.46
5	11	65	0.6	55	58	58.21
6	7	65	1	55	80	78.88
7	5	37.5	0.8	32.5	68	68.46
8	9	92.5	0.4	32.5	70	70.67
9	5	92.5	0.4	32.5	69	68.79
10	3	65	0.6	55	56	54.71
11	9	37.5	0.8	32.5	67	67.33
12	7	65	0.6	55	69	68.83
13	5	92.5	0.4	77.5	54	55.33
14	9	92.5	0.8	77.5	72	73.00
15	9	92.5	0.4	77.5	61	59.96
16	7	10	0.6	55	51	50.71
17	7	65	0.2	55	57	57.04
18	9	37.5	0.8	77.5	60	59.63
19	5	92.5	0.8	32.5	80	81.33
20	7	65	0.6	10	83	82.04
21	7	65	0.6	55	67	68.83
22	7	65	0.6	55	71	68.83
23	7	65	0.6	55	72	68.83
24	9	92.5	0.8	32.5	80	79.96
25	7	65	0.6	55	68	68.83
26	5	92.5	0.8	77.5	72	71.63
27	7	65	0.6	100	61	60.88
28	7	120	0.6	55	74	73.21
29	5	37.5	0.8	77.5	57	58.00
30	7	65	0.6	55	66	68.83

Table 4
Results of ANOVA analysis for the second-order predicted model od DCP adsorption by ZSM-5/M

Parameter	Sum of squares	Average of squares	F Value	p-value
Model	2566.6	183.3	68.6	<0.0001
pH- (A)	18.4	18.4	6.9	0.0192
Contact time- (B)	759.4	759.4	284.2	<0.0001
Adsorbent dose- (C)	715.0	715.0	267.6	<0.0001
DCP concentration- (D)	672.0	672.0	251.5	<0.0001
A×B	0.1	0.1	03.02	0.8805
A×C	10.6	10.6	0.4	0.0654
A×D	7.6	7.6	2.8	0.1132
B×C	14.1	14.1	5.3	0.0366
B×D	0.6	0.6	0.2	0.6530
C×D	14.1	14.1	5.3	0.0366
A^2	262.5	262.5	98.2	<0.0001
B^2	81.0	81.0	30.3	<0.0001
C^2	1.3	1.3	0.5	0.4941
D^2	11.8	11.8	4.4	0.0528
Residual	40.1	2.7		
Lack of Fit	13.3	1.3	0.2	0.9714
R^2	Predictive R^2		Justified R^2	
0.984	0.97		0.955	

Based on obtained results and on the regression between the independent variables and removal efficiency of DCP, an empirical model [Eq. (5)] was obtained to specify the relationship between the independent variables and the response. As seen in the above equation, only the terms that show a significant relationship with the response changes at p-value < 0.05 were included in this predictive model

$$R(\%) = 14.9271 + 11.7179X_1 + 0.3890X_2 + 25.5350X_3 - 0.6294X_4 + 0.1704X_2X_3 + 0.2083X_3X_4 - 0.7734X_1^2 - 0.0023X_2^2 \quad (4)$$

Moreover, Fig. 5 shows the Pareto effect for comparing the effect size of the studied variables on the response. The Pareto effect of each factor on the response was calculated using Eq. (5).

$$P_i = \left[\frac{(b_i^2)}{\sum b_i^2}\right] \times 100 \quad (5)$$

where b is the regression coefficient of each term based on the coded values of the independent variables.

As shown in Fig. 5, the largest effects on response are assigned to pH^2, contact time, adsorbent and adsorbate concentration with values approximately 24.8, 20.5, 19.25, and 18.2%, respectively.

3.6. Effects of pH and contact time on process efficiency

One of the important factors in the adsorption process is the pH variable. The effect of pH on DCP adsorption was studied in the pH range of 3–11. Fig. 6 presents the effects of pH and contact time on adsorption efficiency when DCP concentration was 55 mg/L and ZSM-5/M dose 0.6 g/L. Results show that removal efficiencies were 61.5 and 62.3%, at solution pHs of 3 and 11, respectively, in the 120 min contact time. However, adsorption efficiency rose to 73.2% at solution pH of 7. The largest adsorption took place at pH close to neutral, and adsorption efficiency declined with increases and decreases in pH value. The reported pKa for DCP is 4.09; therefore, half of the DCP surface charge is negative and the other half neutral at pH values equal to pKa, and the negative charge of the adsorbent increases at higher pH values. Moreover, the surface charge of DCP at pH values lower than pKa is neutral [43]. In the experiments, the obtained pHzpc of the adsorbent was about 8.5 (Fig. 7). Therefore, the adsorbent had a negative charge at pH values higher than pHzpc, a positive charge at pH values lower than pHzpc, and a neutral charge at pH value equal to pHzpc. Therefore, it can be concluded that adsorption increases at pH values 4.09–8.5, at which the adsorbent and contaminant have mainly opposite charge. Consequently, increased adsorption in the neutral pH range can result from differences in the surface charge of the adsorbent and adsorbate. Furthermore, reduced efficiencies at acidic and basic pH values could result from the considerably higher H production level at very acidic pH values because H competes with DCP for occupying the adsorbent surface. This is also true in the case of basic pH values because OH^- competes with DCP in occupying the adsorbent surface. In the study by Hammed et al., [39] the best pH for adsorption of methylene blue by ZSM-5 was about 7.Moreover, Pham et al. [44] observed that the nanozeolite synthesized at pH 6 had the highest efficiency in adsorbing the nitrophenyl compound.

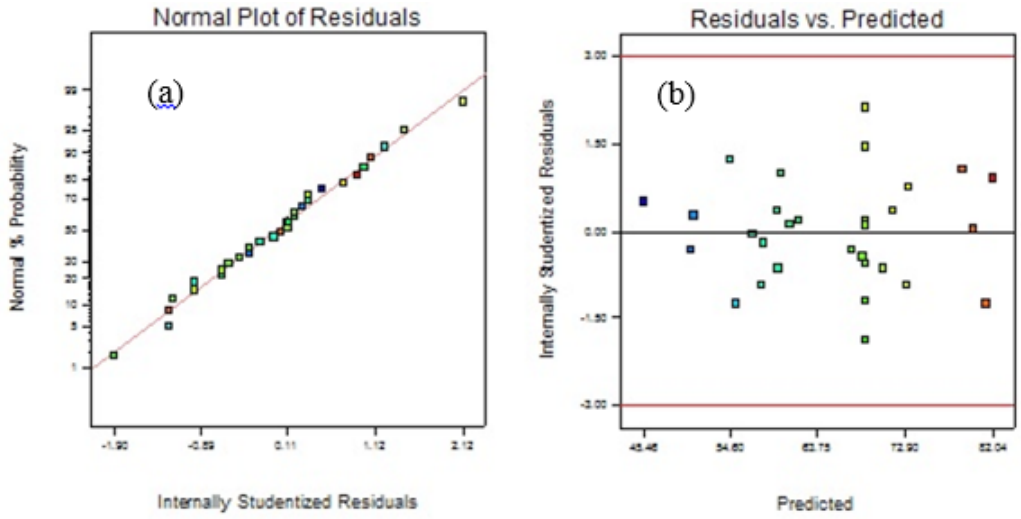

Fig. 5. The normal plot of residuals and plot of residuals vs. predicted values for the developed model.

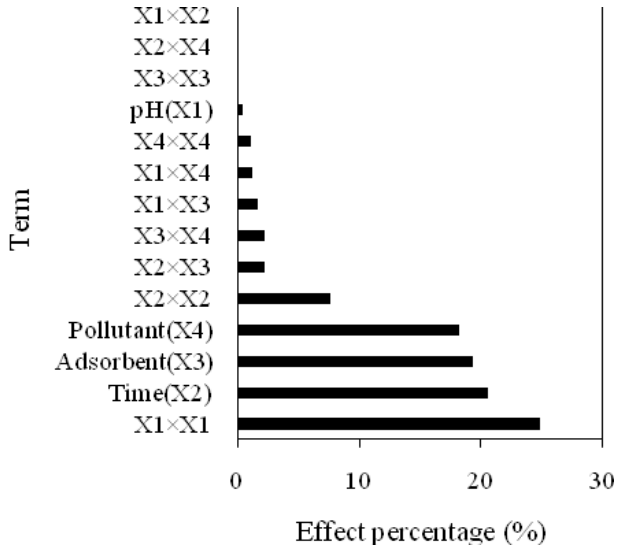

Fig. 6. Pareto chart for DCP adsorption by ZSM-5/M.

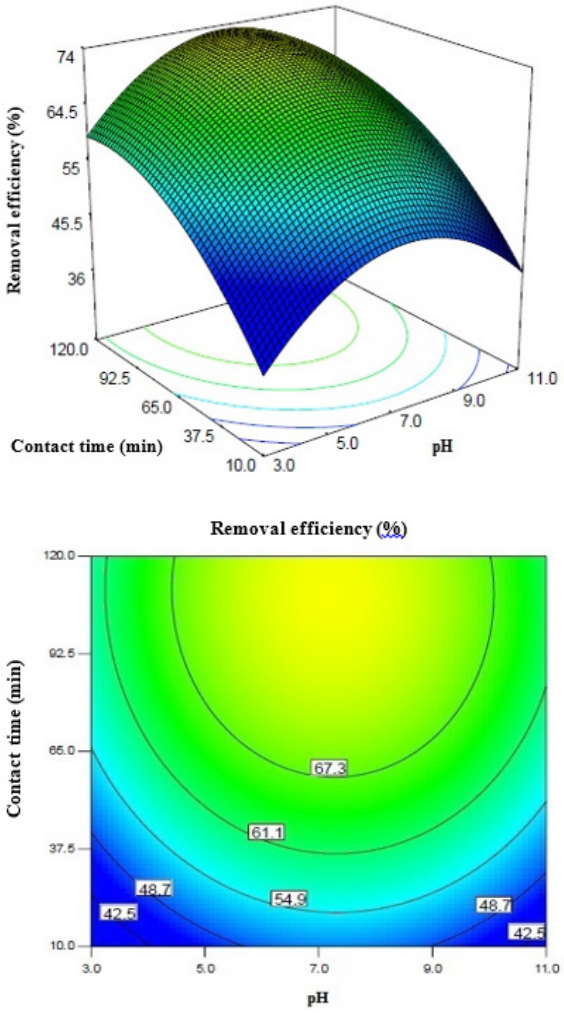

Fig. 7. The effect of contact time and pH on efficiency of DCP adsorption by ZSM-5/M (DCP concentration = 55 mg/L, ZSM-5/M dose = 0.6 g/L).

In the result, it was moreover observed that adsorption efficiencies were 50.7 and 73.2%, respectively, at pH 7 and contact times of 10 and 120 min, respectively. As a result, adsorption efficiency displayed a direct relationship with contact time, and the highest adsorption efficiency was achieved at a contact time of 120 min. However, the adsorption rate declined and changed intangibly at contact times longer than 60 min. The rate of adsorption is high at the beginning of the process because there are unoccupied adsorption sites that can trap contaminant molecules, whereas the unoccupied sites become saturated with the passage of time, leading to lower adsorption rate [33]. Moreover, reduced contaminant concentration, and therefore lower probability for the collision between it and the adsorbent, during longer contact can be considered another case that reduces adsorption rate at longer contact times. Pham et al. [44] showed that the nanozeolite adsorbed the

nitrophenyl compound at higher rate for up to 150 min, and adsorption became almost completed at that time. Therefore, they reported it as the equilibrium time.

3.7. Effect of adsorbent dose and DCP concentration on adsorption efficiency

Fig. 8 shows the effect of adsorbent dose and DCP concentration on adsorption efficiency when pH was 7 and contact time 65 min. Results indicated that removal efficiency improved from about 74 to 88.3% when adsorbent dose increased from 0.2 to 1 g/L at DCP concentration of 10 mg/L. Moreover, adsorption efficiency declined from 88.3 to 74.7% when DCP concentration increased from 10 to 100 mg/L.

Results demonstrated that DCP adsorption increased at higher adsorbent doses. This can be explained by increases in the surfaces and sites available to the adsorbent at higher adsorbent concentrations leading to higher contaminant adsorption efficiencies. However, adsorption sites are rapidly occupied by the contaminant at lower adsorbent doses, thereby lowering adsorption efficiency. Moreover, adsorption capacity declined with increases in adsorbent concentration. This could be due to the reduced collision between adsorbent and contaminant molecules [40]. In agreement with the results of the present research, Mansourian et al. [19] reported that adsorption efficiency is significantly improved with increases in the adsorbent dose.

The effect of initial DCP concentration on adsorption efficiency was also studied. Results indicated that adsorption efficiencies declined with increases in initial DCP concentration. This can be explained as follows. Rapid saturation of the adsorption sites on the surface of the adsorbent takes place with increases in the DCP concentration thereby decreasing adsorption efficiency at the constant adsorbent dosage. Adsorption capacity declined at low DCP concentrations because the collision between adsorbent and DCP molecules declined at low initial DCP concentrations [41]. Azari et al. [34] studied the removal of 2, 4-DCP by magnetic graphene oxide and observed an inverse relationship between adsorption efficiency and contaminant concentration. Wu et al. [47] also found similar results in their research on 2, 4-DCP adsorption by *Phanerochaetechrysosporium* fungal biomass with respect to the effect of the initial concentration of pollutant on adsorption efficiency.

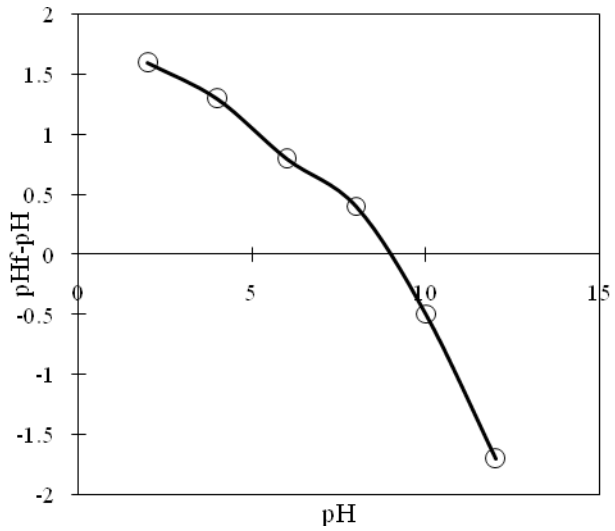

Fig. 8. pHzpc of the ZSM-5/M adsorbent.

3.8. Optimization of the studied factors

Response optimization was used to optimize the studied variables in DCP removal by ZSM-5/M. Since higher removal efficiencies were desired in the present research, the highest removal efficiency was defined as the desired goal. Under these conditions, the optimum variables for pH, contact time, adsorbent dose, and contaminant concentration for reaching the highest adsorption percentage (about 96.1%) were about 6.3, 120 min, 1 g/L, and 10 mg/L (Fig. 9). Three experiments conducted in the optimum lev-

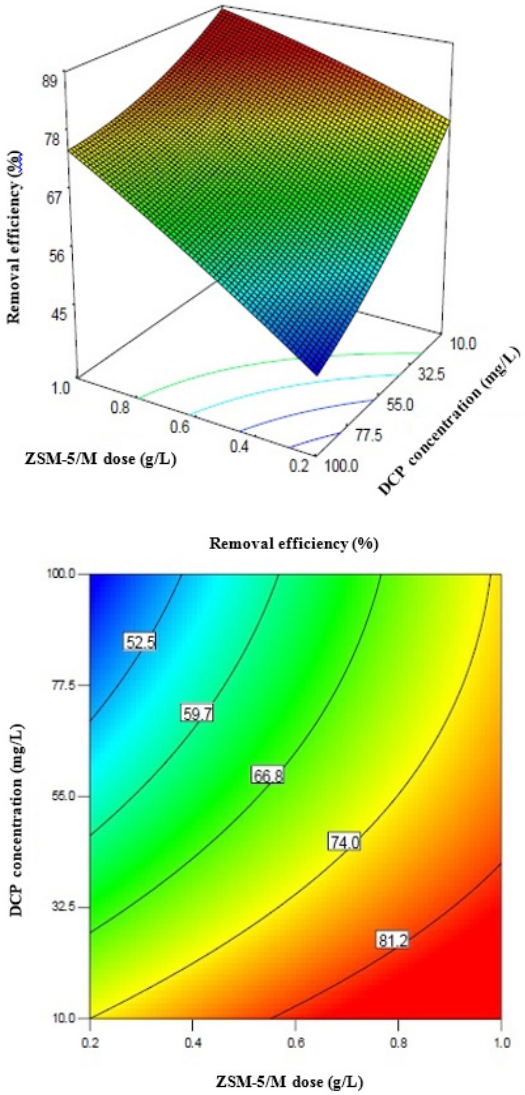

Fig. 9. The effect of DCP concentration and ZSM-5/M dose on the efficiency of DCP adsorption by ZSM-5/M (pH = 7, contact time = 65 min.)

els of the variables were employed to determine the validity of the results predicted by the obtained model. The obtained experimental removals (95% ± 1.4) were so close to the value predicted by the model (96.1%)

3.9. Isotherm studies

Adsorption is described by isotherm equations under normal conditions. These equations help determine contaminant adsorption on the adsorbent, adsorption capacity, and adsorbent surface features. Moreover, adsorption isotherms indicate the relationship between the amount of contaminant adsorbed on the adsorbent and the contaminant concentration in the solution under equilibrium conditions [11,48]. In this research, DCP adsorption on ZSM-5/M was investigated using Freundlich, Langmuir, and Temkin isotherms.

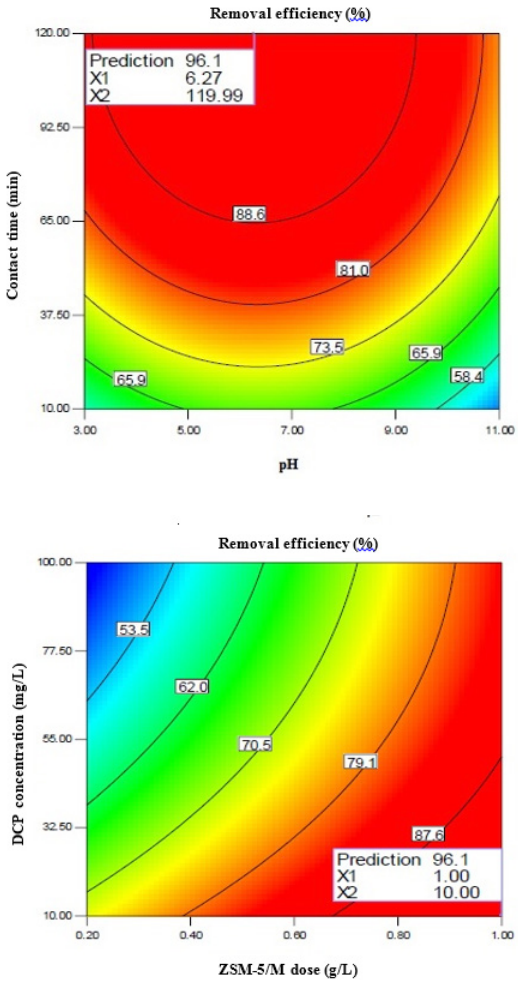

Fig. 10. Efficiency of DCP adsorption by ZSM-5/M under optimum conditions of the studied variables.

3.9.1. Freundlich isotherm

If the adsorption isotherm follows Freundlich isotherm, it means that adsorption takes place on a heterogeneous surface of a multilayer adsorbent and interactions take place between adsorbent molecules during the adsorption process. Moreover, this isotherm shows that the adsorption energy of the adsorbing centers declines during the adsorption process [19]. The linear form of Freundlich isotherm is presented in Eq. (6).

$$\ln q_e = \ln K_f + \frac{1}{n}\ln C_e \tag{6}$$

where q_e is the amount of the contaminant adsorbed per gram of the adsorbent (mg/g) under equilibrium conditions, C_e the contaminant concentration at equilibrium, K_f the Freundlich constant and a relative indicator of adsorption capacity (mg/g), and n indicates adsorption intensity. A large value for n shows desirability of the adsorption process. Values of Ln (q_e) were plotted against those of Ln (C_e) to determine the linear equation of this isotherm. Values of n greater than 1 indicate the suitability and favorability of the adsorption, equal to 1 show that the adsorption process is linear, and smaller than 1 demonstrate that adsorption is chemical. If values of n are greater than, they show that the adsorption process is a favorable physical one. $1/n$ shows the heterogeneity factor of the adsorption. If the value of this factor is in the 0–1 range, adsorption is heterogeneous, if it is less than zero adsorption is homogeneous, and if it is greater than 1 adsorption is a combination of homogeneous/heterogeneous conditions [8,49]. Results (Table 5) indicated that the R^2 value for the Freundlich isotherm was higher compared to the other isotherms. Therefore, the adsorption process followed this isotherm.

3.9.2. Langmuir isotherm

This isotherm is used to study adsorption on a homogeneous surface. There is no interaction between the adsorbed molecules in the adsorption processes following this isotherm. It is assumed that adsorption energy is uniformly

Table 5
Information of kinetic and isotherm models for the adsorption of DCP over ZSM-5/M adsorbent

Temkin isotherm			Freundlich isotherm			Langmuir isotherm		
K_T	B_1	R^2	K_F	n	R^2	q_{max}	K_L	R^2
1.47	16.67	0.9631	5.52	1.53	0.9967	87.72	0.0474	0.9786
Pseudo-first order kinetic			Pseudo-second order kinetic			Inter-particle penetration kinetic		
q_e	K_1	R^2	q_e	K_2	R^2	K_p	R^2	q_{exp}
6.59	0.0265	0.9996	4.96	0.0217	0.4612	5.28	0.9793	12

distributed on the adsorbent surface, adsorption takes place in a single layer, and most of the adsorption depends on the saturation level of the single adsorption layer [50]. Eq. (7) presents the linear form of Langmuir isotherm.

$$\frac{1}{q_e} = \frac{1}{q_m} + \frac{1}{K_L q_m}\left(\frac{1}{C_e}\right) \tag{7}$$

where C_e is the contaminant concentration at equilibrium (mg/L), q_e the amount of contaminant adsorbed per gram of the adsorbent (mg/g), q_m the maximum adsorption capacity of the single adsorption layer (mg/g), and K_L the Langmuir constant (L/mg) [51]. Values of $1/q_e$ were plotted against those of $1/C_e$ to draw the diagram and obtain the linear equation. Information of Langmuir isotherm is reported in Table 5. The maximum adsorption capacity obtained from Langmuir isotherm was calculated as 87.7 mg/g in the optimum values of pH = 6.3, contact time = 120 min, and adsorbent dose = 1 g/L. However, Langmuir isotherm corresponded to the experimental data, R^2 of the isotherm was obtained lower values compared to that of Freundlich isotherm.

3.9.3. Temkin isotherm

Temkin isotherm, another model that reveals how adsorption takes place, was studied in this research. This model assumes that heat absorption of all molecules in the adsorption layer decreases when the adsorption layer is occupied due to the interactions between the adsorbent and the adsorbate and the heat reduction is linear. Adsorption in this isotherm is described as uniform distribution of binding energies [52]. The Temkin isotherm that is usually used in studies is in the linear form of Eq. (8).

$$q_e = B_1 \ln K_T + B_1 \ln C_e \tag{8}$$

In the Temkin model, C_e is the contaminant concentration at equilibrium (mg/L), q_e the amount of contaminant adsorbed per gram of adsorbent (mg/g), B_1 is a constant related to the heat of adsorption, and K_T is the equilibrium binding constant (L/g). Values of $1/q_e$ were plotted against those of $1/C_e$ to draw the diagram and determine the linear equation. As for the model fitting the experimental data, this model yielded poorer fitness or lower R^2 value (Table 5) compared to Freundlich isotherm.

3.10. Kinetic studies

Pseudo-first-order and pseudo-second order and inter-particle penetration kinetic equations were used to study mechanisms that control the adsorption process like mass transfer and chemical reactions and to determine adsorption rate.

3.10.1. Pseudo-first order kinetic model

This model, developed by Lagergren, is used for liquid/solid adsorption systems [49]. It shows that penetration happens from inside a layer and is based on the capacity of the solid in which changes in adsorption rate with the passage of time are related to the number of unoccupied adsorptive sites on the adsorbent surface. The linear form of this model is presented in Eq. (9).

$$\ln\left(q_e - q_t\right) = \ln q_e - K_1 t \tag{9}$$

In this equation, q_e and q_t are the amount of contaminant adsorbed per gram of the adsorbent (mg/g) at equilibrium and at time t, respectively, and K_1 the pseudo-first order kinetic model adsorption rate constant (min^{-1}). The values of ln ($q_e - q_t$) were plotted against those of t to draw the diagram and determine the linear form of the pseudo-first order kinetic model. Results (Table 5) indicate that the value of the R^2 coefficient in this method is higher than other kinetic models, and the differences between the experimental q values and the q values obtained in this model are smaller compared to the pseudo-second-order kinetic model. These results indicate that this model is fitted the laboratory data better.

3.10.2. Pseudo-second-order kinetic model

Adsorption kinetics was also studied using pseudo-second-order kinetic model. The pseudo-second-order kinetic model assumes that the adsorption process follows a second-order chemical adsorption. The chemical adsorption is limiting step of adsorption rate and controlling step of adsorption processes, and is the basis for the adsorption of the solid phase in which the rate of occupation of the adsorptive sites is proportional to the square of the number of unoccupied sites [49]. This model has a linear form presented in Eq. (10).

$$\frac{t}{q_t} = \frac{1}{k_2 {q_e}^2} + \frac{1}{q_e} t \tag{10}$$

where q_e and q_t are the amount of contaminant adsorbed per gram of the adsorbent (mg/g) at equilibrium and at time t, respectively, and K_2 the pseudo-second-order kinetic model adsorption rate constant (g/mg·min). The values of t/q_t were plotted against those of t to draw the diagram and determine the linear form of the pseudo-second-order kinetic model. Results indicate that the value of the R^2 coefficient in this method is smaller than other models, and this model is weaker than the pseudo-first-order kinetic model in fitting experimental data.

3.10.3. Inter-particle penetration model

The inter-particle penetration model is another common model for kinetic evaluation of adsorption processes. This model is based on a phenomenon in which analyte adsorption on the adsorbent takes place in four stages: Migration of analyte molecules from the matrix of the solution to the adsorbent surface through mass penetration, penetration of analyte molecules through the boundary layer to the adsorbent surface through layer penetration, transfer of analyte molecules from the surface to the internal pores of the adsorbent through the inter-particle penetration mechanism or pore penetration, and adsorption of the species on adsorbent surface

by chemical reaction through ion exchange, complexation, and chelation [53]. The linear form of this model is presented in Eq. (11).

$$q_t = K_p t^{0.5} + C \tag{11}$$

where q_t is the amount of contaminant adsorbed per gram of the adsorbent at time t, K_p the constant of inter-particle penetration rate (mg/g·min$^{1/2}$), and C is the y-intercept. Values of q_t were plotted against those of $t^{0.5}$ to draw the diagram and determine the linear equation of inter-particle penetration kinetics. Results show that the R^2 coefficient in this model is smaller compared to the pseudo-first order kinetic model and larger than that of the pseudo-second-order kinetic model.

3.11. Thermodynamic study

Thermodynamic study for the adsorption process was performed at the optimum condition of the independent variable, at 20, 30 and 40°C temperatures of the samples. The thermodynamic study determined the parameters, including enthalpy change (ΔH°, kJ/mol), entropy change (ΔS°, J/mol/K), and the change of free Gibbs energy (ΔG°, kJ/mol) [52,54].

Eq. (12) was applied to determine ΔG° parameter

$$\Delta G^{\circ} = -RT \ln K_d \tag{12}$$

where R is devoted to the gas constant (8.314J/mol·K), T denotes the solution temperature (K) and K_d is assigned to the distribution coefficient determined by the following equation:

$$K_d = q_e / C_e \tag{13}$$

Here q_e (mg/g) and C_e (mg/L) present the adsorption capacity and adsorbate concentration in the equilibrium, respectively. Based on Eq. (14), the parameters of ΔH° and ΔS° were determined by plotting $1/T \times 10^{-3}$ vs. ln K_d. The information related to the thermodynamic model has been summarized in Table 6. The negative values of ΔG° confirmed spontaneous adsorption to occur. On the other hand, the ΔG° value was observed to decline at the elevated temperatures, indicating spontaneous adsorption reduction and undesirability of the process with increasing temperature. The negative values of ΔH° specify the exothermic nature of the process adsorption, and the decrease of efficiency at the higher temperatures. The negative values of ΔS° demonstrate the randomness at the ZSM-5/M-solution interface during the adsorption.

$$\ln K_d = \frac{\Delta S^{\circ}}{R} - \frac{\Delta H^{\circ}}{RT} \tag{14}$$

3.12. Comparison of ZSM-5/M with various adsorbents

Table 5 compares the maximum adsorption capacity of the ZSM-5/M with that of some other adsorbents previously studied. It is clearly observed that the ZSM-5/M composite in the present study has a considerable adsorption capacity as compared with that of the other adsorbents.

4. Conclusion

In recent years, several studies have done to develop and use new, efficient, and low-cost adsorbents instead of commercial adsorbents like activated carbon for the removal of pollutants from aqueous environments. In the present research, DCP adsorption by ZSM-5/M was investigated in aqueous solution. Among studied variables, the highest influence percentage on the adsorption process was assigned to the square-order effect of pH. Moreover, under optimum conditions of the variables, pH = 6.3, contact time = 120 min, adsorbent dose = 1 g/L, and contaminant concentration = 10 mg/L, the highest adsorption efficiency, and adsorption capacity were achieved as about 96.1% and 87.7 mg/g, respectively. It also observed that the adsorption process has a spontaneous and exothermic nature, and the experimental data were described better by Freundlich isotherm and pseudo-first order kinetic. ZSM-5/M as compared with other absorbents in other research indicates the considerable efficiency and good adsorption. Given the high efficiency, suitable adsorption capacity, low cost, and ease of adsorbent separation after the adsorption process, we can potentially suggest ZSM-5/M as a suitable alternative for removal of DCP and other similar contaminants.

Acknowledgement

This study is the result of a research project with Grant Number: 196197. The authors of the study would like to extend their sincere gratitude to Isfahan University of Medical Sciences for its assistance in conducting the research.

Table 6
Thermodynamic information of DCP adsorption process using ZSM-5/M

Pollutant (mg/L)	$\Delta G\left(kJmol^{-1}\right)$			$\Delta S^{\circ}\left(Jmol^{-1}K^{-1}\right)$	$\Delta H^{\circ}\left(kJ\ mol^{-1}\right)$	R^2
	293 °K	303°K	313°K			
15	–7642	–3877	–2956	–239.41	–79.16	0.9436
30	–3990	–2888	–1730	–160.74	–47.44	0.9984
45	–3232	–2215	–880	–142.88	–42.43	0.9954
60	–2156	–1331	–228	–131.65	–37.86	0.9933

Table 7
Comparison of adsorption capacity of ZSM-5/M with some various adsorbents

Adsorbent	Adsorption capacity (mg/g)		Ref.
Bentonite nanoparticles	58.21		[54]
Montmorillonite nanoparticles	48.2		
Activated carbon	0.002 mol/g		[55]
Beta zeolite (Si/Al = 43)	0.00072 mol/g		
HZSM-5 zeolite (Si/Al = 15)	0.00022 mol/g		
HZSM-5 zeolite (Si/Al = 40)	0.00032 mol/g		
HZSM-5 zeolite (Si/Al = 140)	0.00051 mol/g		
CuZSM-5 zeolite (Si/Al = 15)	0.00028 mol/g		
ZSM-5	141.8		[56]
Chitin/ZSM-5	1217.3		
Zeolite–rGO	48.6		[57]
Extracted chitin from shrimp shell	116.07		[51]
Bentonite nanoparticles	Reactive Yellow 15	156.9	[58]
	Reactive Yellow 42	170.7	
Oil shale ash	Deltamethrin	11.4	[59]
	Lambda-Cyhalothrin	8.6	
Bentonite modified with benzyldimethyltetradecylammonium chloride	35		[60]
Bentonite composite with Eriobotrya japonica seeds	58.87		[61]
Modified chitosan	10		[62]
Cross-linked chitosan beads	249.8		[63]
ZSM-5/M	87.7		Present study

References

[1] J.A. Mota, R.A. Chagas, E.F. Vieira, A.R. Cestari, Synthesis and characterization of a novel fish scale-immobilized chitosan adsorbent—Preliminary features of dichlorophenol sorption by solution calorimetry, J. Hazard. Mater., 229 (2012) 346–353.

[2] M. Abbas, M. Adil, S. Ehtisham-ul-Haque, B. Munir, M. Yameen, A. Ghaffar, G. AbbasShar, M.Asif Tahir, M. Iqbal, Vibrio fischeri bioluminescence inhibition assay for ecotoxicity assessment: A review, Sci. Total Environ., 626 (2018) 1295–1309.

[3] M. Iqbal, Vicia faba bioassay for environmental toxicity monitoring: a review, Chemosphere, 144 (2016) 785–802.

[4] I. Hussain, Y. Zhang, S. Huang, X. Du, Degradation of p-chloroaniline by persulfate activated with zero-valent iron, Chem. Eng. J., 203 (2012) 269–276.

[5] R. Li, X. Jin, M. Megharaj, R. Naidu, Z. Chen, Heterogeneous Fenton oxidation of 2, 4-dichlorophenol using iron-based nanoparticles and persulfate system, Chem. Eng. J., 264 (2015) 587–594.

[6] M. Raoov, S. Mohamad, M.R. Abas, Removal of 2, 4-dichlorophenol using cyclodextrin-ionic liquid polymer as a macroporous material: characterization, adsorption isotherm, kinetic study, thermodynamics, J. Hazard. Mater., 263 (2013) 501–516.

[7] F. Shaarani, B. Hameed, Batch adsorption of 2, 4-dichlorophenol onto activated carbon derived from agricultural waste, Desalination, 255 (2010) 159–164.

[8] A. Nasser, U. Mingelgrin, Birnessite-induced mechanochemical degradation of 2,4-dichlorophenol, Chemosphere, 107 (2014) 175–179.

[9] J.B. Quintana, R. Rodil, S. Muniategui-Lorenzo, P. López-Mahía, D. Prada-Rodríguez, Multiresidue analysis of acidic and polar organic contaminants in water samples by stir-bar sorptive extraction–liquid desorption–gas chromatography–mass spectrometry, J. Chromatogr. A, 1174 (2007) 27–39.

[10] S.K. Nadavala, K. Swayampakula, V.M. Boddu, K. Abburi, Biosorption of phenol and o-chlorophenol from aqueous solutions on to chitosan–calcium alginate blended beads, J. Hazard. Mater., 162(1) (2009) 482–489.

[11] M. Moradi, M. Soltanian, M. Pirsaheb, K. Sharafi, S. Soltanian, A. Mozafari, The efficiency study of pumice powder to lead removal from the aquatic environment: isotherms and kinetics of the reaction, JMUMS, 23 (2014) 64–75.

[12] M. Moradi, A.M. Mansouri, N. Azizi, J. Amini, Karimi K, K. Sharafi, Adsorptive removal of phenol from aqueous solutions by copper (cu)-modified scoria powder: process modeling and kinetic evaluation, Desal. Water Treat., 57 (2016) 11820–11834.

[13] M. Heydari, K. Karimyan, M. Darvishmotevalli, A. Karami, Y. Vasseghian, N. Azizi, Data for efficiency comparison of raw pumice and manganese-modified pumice for removal phenol from aqueous environments—Application of response surface methodology, Data in Brief., 20 (2018) 942–954.

[14] M. Moradi, M. Heydari, M. Darvishmotevalli, K. Karimyan, V.K. Gupta, Y. Vasseghian, Kinetic and modeling data on phenol removal by Iron-modified Scoria Powder (FSP) from aqueous solutions, Data in Brief., 20 (2018) 957–968.

[15] G. Bayramoglu, I. Gursel, Y. Tunali, M.Y. Arica, Biosorption of phenol and 2-chlorophenol by Funalia trogii pellets, Bioresour. Technol., 100(10) (2009) 2685–2691.

[16] M. Moradnia, M.M. Emamjomeh, An environmental-friendly study on sanitary wastewater treatment for small community, Desal. Water Treat., 94 (2017) 25–30.

[17] S. Shen, J. Ren, J. Chen, X. Lu, C. Deng, X. Jiang, Development of magnetic multiwalled carbon nanotubes combined with near-infrared radiation-assisted desorption for the determination of tissue distribution of doxorubicin liposome injects in rats, J. Chromatogr. A, 1218(29) (2011) 4619–4626.

[18] M.M. Emamjomeh, H.A. Jamali, M. Moradnia, S. Mousavi, Z. Karimi, Sanitary wastewater treatment using combined anaerobic and phytoremediation systems, JMUMS, 26(138)(2016) 140–150.
[19] N. Mansourian, G. Javedan, M. Darvishmotevalli, K. Sharafi, H.R. Ghaffari, H. Sharafi, H. Arfaeinia, M. Moradi, Efficiency evaluation of zeolite powder, asan adsorbent for the removal of nickel and chromium from aqueous solution: Isotherm and kinetic study, Int. J. Pharm. Technol., 8(2) (2016) 13891–13907.
[20] H.M.F. Freundlich, Uber die adsorption in losungen, J. Phys. Chem., 57 (1906) 385–470.
[21] M.M. Kalhor, A.A. Rafati, L. Rafati, A.A. Rafati, Synthesis, characterization and adsorption studies of amino functionalized silica nano hollow sphere as an efficient adsorbent for removal of imidacloprid pesticide, J. Mol. Liq., 266 (2018) 453–459.
[22] M. Kamranifar, M. Khodadadi, V. Samiei, B. Dehdashti, M.N. Sepehr, L. Rafati, N. Nasseh, Comparison the removal of reactive red 195 dye using powder and ash of barberry stem as a low cost adsorbent from aqueous solutions: Isotherm and kinetic study, J. Mol. Liq., 255 (2018) 572–577.
[23] L. Rafati, M. Ehrampoush, A. Rafati, M. Mokhtari, A. Mahvi, Removal of ibuprofen from aqueous solution by functionalized strong nano-clay composite adsorbent: kinetic and equilibrium isotherm studies, Int. J. Environ. Sci. Technol., 15(3) (2018) 513–524.
[24] L. Rafati, M.H. Ehrampoush, A.A. Rafati, M. Mokhtari, A.H. Mahvi, Modeling of adsorption kinetic and equilibrium isotherms of naproxen onto functionalized nano-clay composite adsorbent, J. Mol. Liq., 224 (2016) 832–841.
[25] L. Rafati, R. Nabizadeh, A.H. Mahvi, M.H. Dehghani, Removal of phosphate from aqueous solutions by iron nano-particle resin Lewatit (FO36), Korean J. Chem. Eng., 29(4) (2012) 473–477.
[26] L. Rafati, M.H. Ehrampoush, A.A. Rafati, M. Mokhtari, A.H. Mahvi, Nanocomposite adsorbent based on β-cyclodextrin-PVP-clay for the removal of naproxen from aqueous solution: Fixed-bed column and modeling studies, Desal. Water Treat., 132 (2018) 63–74.
[27] A. Abourriche, H. Hannache, M. Oumam, Elaboration of novel adsorbent from Moroccan oil shale using Plackett–Burman design, Chemistry Int., 4 (2018) 7–14.
[28] S. Boumaza, A. Yenounne, W. Hachi, F. Kaouah, Y. Bouhamidi, M. Trari, application of Typha angustifolia (L.) dead leaves waste as biomaterial for the removal of cationic dye from aqueous solution, Int. J. Environ. Res., 12(5) (2018) 561–573.
[29] Z. Al-Qodah, A. Shawaqfeh, W. Lafi, Two-resistance mass transfer model for the adsorption of the pesticide deltamethrin using acid treated oil shale ash, Adsorption, 13(1) (2007) 73–82.
[30] Z. Al-Qodah, W.K. Lafi, Z. Al-Anber, M. Al-Shannag, A. Harahsheh, Adsorption of methylene blue by acid and heat treated diatomaceous silica, Desalination, 217 (2007) 212–224.
[31] B. Koubaissy, G. Joly, I. Batonneau-Gener, P. Magnoux, Adsorptive removal of aromatic compounds present in wastewater by using dealuminated Faujasite zeolite, Ind. Eng. Chem. Res., 50(9) (2011) 5705–5713.
[32] R.I. Yousef, B. El-Eswed, H. Ala'a, Adsorption characteristics of natural zeolites as solid adsorbents for phenol removal from aqueous solutions: kinetics, mechanism, and thermodynamics studies, Chem. Eng. J., 171(3) (2011) 1143–1149.
[33] S. Wang, Z. Zhu, Characterisation and environmental application of an Australian natural zeolite for basic dye removal from aqueous solution, J. Hazard. Mater., 136 (2006) 946–952.
[34] A. Azari, M. Salari, M.H. Dehghani, M. Alimohammadi, H. Ghaffari, K. Sharafi, N. Shariatifar, M. Baziar, Efficiency of magnitized graphene oxide nanoparticles in removal of 2, 4-dichlorophenol from aqueous solution, J. Mazandaran Univ. Med. Sci., 26(144) (2017) 265–281.
[35] G. Asgari, M. Salari, Optimized synthesis of carbon-doped nano-MgO and its performance study in catalyzed ozonation of humic acid in aqueous solutions: Modeling based on response surface methodology, J. Environ. Manage., 239 (2019) 198–210.
[36] M.M. Emamjomeh, H.A. Jamali, M. Moradnia, Optimization of nitrate removal efficiency and energy consumption using a batch monopolar electrocoagulation: Prediction by RSM method, J. Environ. Eng., 143(7) (2017) 04017022.
[37] S. Taherkhani, M. Darvishmotevalli, K. Karimyan, B. Bina, A. Fallahi, H. Karimi, Dataset on photodegradation of tetracycline antibiotic with zinc stannate nanoflower inaqueous solution–Application of response surface methodology, Data in Brief. 19 (2018) 1997–2007.
[38] Z. Wan, W. Wu, W. Chen, H. Yang, D. Zhang, Direct synthesis of hierarchical ZSM-5 zeolite and its performance in catalyzing methanol to gasoline conversion, Ind. Eng. Chem. Res., 53(50) (2014) 19471–19478.
[39] A.K. Hammed, N. Dewayanto, D. Du, M.H. Ab Rahim, M.R. Nordin, Novel modified ZSM-5 as an efficient adsorbent for methylene blue removal, J. Environ. Chem. Eng., 4(3) (2016) 2607–2616.
[40] P. Daraei, S.S. Madaeni, N. Ghaemi, E. Salehi, M.A. Khadivi, R. Moradian, et al., Novel polyethersulfone nanocomposite membrane prepared by PANI/Fe_3O_4 nanoparticles with enhanced performance for Cu (II) removal from water, J. Membr. Sci., 415 (2012) 250–259.
[41] L. Pislaru-Danescu, A. Morega, G. Telipan, V. Stoica, Nanoparticles of ferrofluid Fe_3O_4 synthetised by coprecipitation method used in microactuation process, Optoelectron. Adv. Mater., 4(8) (2010) 1182–1186.
[42] M. Moradi, F. Ghanbari, M. Manshouri, K.A. Angali, Photocatalytic degradation of azo dye using nano-ZrO_2/UV/persulfate: Response surface modeling and optimization, Korean J. Chem. Eng., 33(2) (2016) 539–546.
[43] W. Jianlong, Q. Yi, N. Horan, E. Stentiford, Bioadsorption of pentachlorophenol (PCP) from aqueous solution by activated sludge biomass, Bioresour. Technol., 75(2) (2000) 157–161.
[44] T.-H. Pham, B.-K. Lee, J. Kim, Improved adsorption properties of a nano zeolite adsorbent toward toxic nitrophenols, Process. Saf. Environ., 104 (2016) 314–322.
[45] M.A. Zazouli, D. Balarak, Y. Mahdavi, M. Ebrahimi, Adsorption rate of 198 reactive red dye from aqueous solutions by using activated red mud, Iran. J. Health Sci., 1 (2013) 36–43.
[46] S.-L. Hii, S.-Y. Yong, C.-L. Wong, Removal of rhodamine B from aqueous solution by sorption on Turbinaria conoides (Phaeophyta), J. Appl. Phycol., 21(5) (2009) 625–631.
[47] J. Wu, H.-Q. Yu, Biosorption of 2, 4-dichlorophenol from aqueous solution by Phanerochaete chrysosporium biomass: Isotherms, kinetics and thermodynamics, J. Hazard. Mater., 137 (2006) 498–508.
[48] J.-M. Li, X.-G. Meng, C.-W. Hu, J. Du, Adsorption of phenol, p-chlorophenol and p-nitrophenol onto functional chitosan, Bioresour. Technol., 100(3) (2009) 1168–1173.
[49] P.S. Kumar, S. Ramalingam, C. Senthamarai, M. Niranjanaa, P. Vijayalakshmi, S. Sivanesan, Adsorption of dye from aqueous solution by cashew nut shell: Studies on equilibrium isotherm, kinetics and thermodynamics of interactions, Desalination, 261 (2010) 52–60.
[50] B. Alyüz, S. Veli, Kinetics and equilibrium studies for the removal of nickel and zinc from aqueous solutions by ion exchange resins, J. Hazard. Mater., 167(1–3) (2009) 482–488.
[51] I. Langmuir, The constitution and fundamental properties of solids and liquids, Anal. Chem. Soc., 38 (1916) 221–295.
[52] A. Naghizadeh, F. Ghasemi, E. Derakhshani, H. Shahabi, Thermodynamic, kinetic and isotherm studies of sulfate removal from aqueous solutions by graphene and graphite nanoparticles, Desal. Water Treat., 80 (2017) 247–254.
[53] R. Ocampo-Pérez, R. Leyva-Ramos, E. Padilla-Ortega, Equilibrium and kinetic adsorption of organic compounds onto organobentonite: application of a surface diffusion model, Adsorpt. Sci. Technol., 29(10) (2011) 1007–1024.
[54] E. Derakhshani, A. Naghizadeh, Optimization of humic acid removal by adsorption onto bentonite and montmorillonite nanoparticles, J. Mol. Liq., 259 (2018) 76–81.
[55] L. Damjanović, V. Rakić, V. Rac, D. Stošić, A. Auroux, The investigation of phenol removal from aqueous solutions by zeolites as solid adsorbents, J. Hazard. Mater., 184(1) (2010) 477–484.

[56] G.V. Brião, S.L. Jahn, E.L. Foletto, G.L. Dotto, Adsorption of crystal violet dye onto a mesoporous ZSM-5 zeolite synthetized using chitin as template, J. Colloid Interface Sci., 508 (2017) 313–322.
[57] J. Zhu, Y. Wang, J. Liu, Y. Zhang, Facile one-pot synthesis of novel spherical zeolite–reduced graphene oxide composites for cationic dye adsorption, Ind. Eng. Chem. Res., 53(35) (2014) 13711–13717.
[58] A. Naghizadeh, M. Kamranifar, A.R. Yari, M.J. Mohammadi, Equilibrium and kinetics study of reactive dyes removal from aqueous solutions by bentonite nanoparticles, Desal. Water Treat., 97 (2017) 329–337.
[59] Z. Al-Qodah, A.T. Shawaqfeh, W.K. Lafi, Adsorption of pesticides from aqueous solutions using oil shale ash, Desalination, 208 (2007) 294–305.
[60] S. Ghezali, A. Mahdad-Benzerdjeb, M. Ameri, A.Z. Bouyakoub, Adsorption of 2,4,6-trichlorophenol on bentonite modified with benzyldimethyltetradecylammonium chloride, Chemistry Int., 4 (2018) 24–32.
[61] M. Mushtaq, H.N. Bhatti, M. Iqbal, S. Noreen, Eriobotrya japonica seed biocomposite efficiency for copper adsorption: isotherms, kinetics, thermodynamic and desorption studies, J. Environ. Manage., 176 (2016) 21–33.
[62] A. Naghizadeh, R. Nabizadeh, Removal of reactive blue 29 dye by adsorption on modified chitosan in the presence of hydrogen peroxide, Environ. Prot. Eng., 42(1) (2016) 149–168.
[63] M.-S. Chiou, P.-Y. Ho, H.-Y. Li, Adsorption of anionic dyes in acid solutions using chemically cross-linked chitosan beads, Dyes Pigm., 60(1) (2004) 69–84.